Evaluation of the cooling trend in the ionosphere using functional regression with incomplete curves

Oleksandr Gromenko
Department of Mathematics, Tulane University, New Orleans, LA 70118
Piotr Kokoszka
Department of Statistics, Colorado State University, Fort Collins, CO 80523
Jan Sojka
Department of Physics, Utah State University, Logan UT, 84322

Abstract

Long term trends in the ionosphere can impact the operation of space–based civilian and defense systems. The ionospheric cooling trend studied in this paper is also related to the global warming hypothesis; both are attributed to the same driver, namely the increased concentration of greenhouse gasses. The hypothesis that a cooling trend in the ionosphere exists has been an important focus of space physics research for over two decades. A central difficulty in reaching broadly agreed on conclusions has been the absence of data with sufficiently long temporal and sufficiently broad spatial coverage. Complete time series of data that cover several decades exist only in a few separated (industrialized) regions. The space physics community has struggled to combine the information contained in these data, and often contradictory conclusions have been reported based on the analyses relying on one or a few locations. We present a statistical analysis that uses all data, even those with incomplete temporal coverage. It is based on a new functional regression approach that can handle spatially indexed curves whose temporal domain depends on location and may contain gaps. We conclude that a statistically significant cooling trend exists in the Northern Hemisphere. This confirms the hypothesis put forward in the space physics community over two decades ago.

KEY WORDS: Cooling trend; Functional regression; Incomplete time series; Ionosphere, Solar activity, Spatial averaging; Spatio–temporal modeling.

1 Introduction

This paper is concerned with a long standing problem of space physics research. The increased concentration of greenhouse gases in the upper atmosphere is associated with global warming in the lower troposphere. Roble and Dickinson (1989) suggested that the increasing amounts of these radiatively active gases, mostly CO_2 and CH_4, would lead to a global cooling in the thermosphere. Rishbeth (1990) pointed out that this would result in a thermal contraction of the atmosphere and the global lowering of the ionospheric peak height and the decrease of the ionospheric peak density, see Fig. 1. The F region peak has

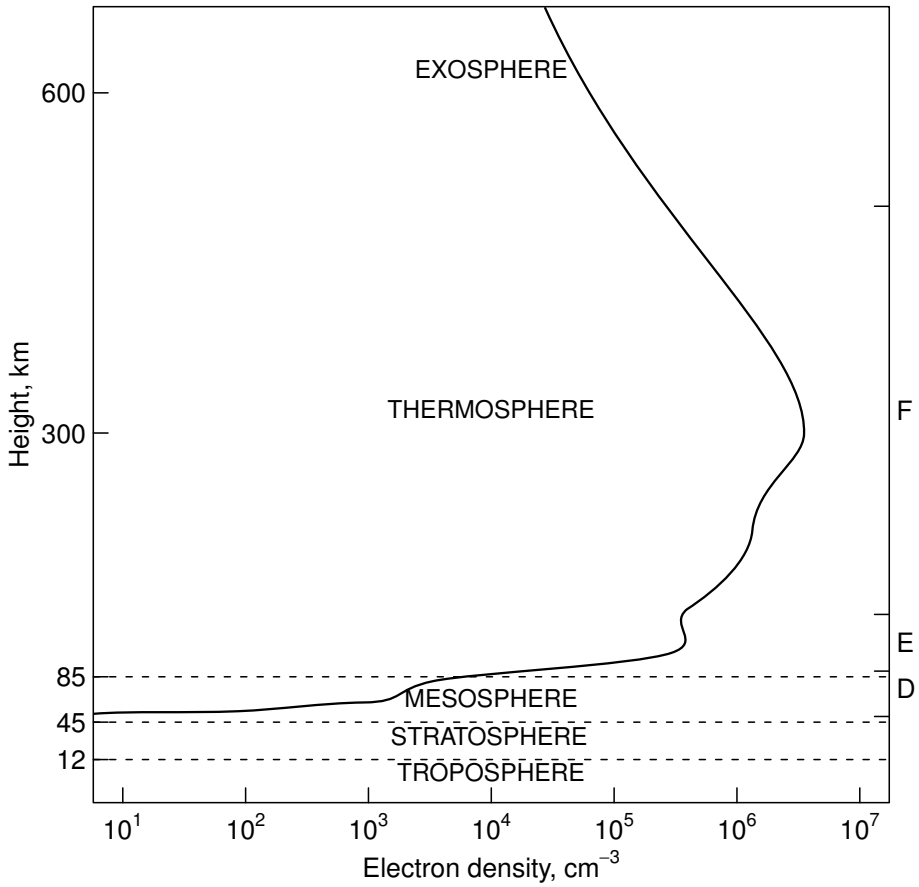

Figure 1: Typical profile of day time ionosphere. The curve shows electron density as a function of height. The right vertical axix indicates the D, E and F regions of the ionosphere.

been observed for many decades by globally distributed ground–based ionosondes. The ionosonde is a type of radar projecting a spectrum of high-frequencies (HF) vertically into the ionosphere. In principle, these observations could be used to quantitatively test the hypothesis of Roble and Dickinson (1989). A long term change in the ionosphere can impact space–based navigation (including GPS systems), HF (2-30MHz) radio communication and the operation of low orbit satellites. It is associated with the global warming hypothesis because a physical mechanism for the conjectured cooling trend is also attributable to greenhouse gases.

The ionospheric layer which contains the peak electron density is known as the F2 region (the right–most peak in Fig. 1). Ionosonde measurements allow us to observe a critical frequency, denoted foF2, which is related to the height of the F2 region peak. There has been extensive space physics research aimed at determining if a decreasing temporal trend in the foF2 frequency indeed exists. Lastovicka *et al.* (2008) review some of the relevant literature. Long-term changes in the ionosphere are usually described using a

linear approximation referred to as the trend. The main problem in its determination is the separation of the solar activity; the solar cycle dominates the shape of the foF2 curves, see Fig. 2. A comprehensive overview of statistical methods proposed in the space physics community is given in Lastovicka *et al.* (2006). The main problem from which they suffer is their inability to combine the information from many spatial locations. The usual approach is to calculate trends separately at a number of locations, often using different time periods, and then average these trends to obtain a sense of a global trend, see Bremer *et al.* (2012) and Mielich and Bremer (2013) for a recent contribution and a discussion of previous work. There has, however, long been a sentiment in the ionospheric physics community, that, in addition to informative exploratory analyses, an inferential statistical framework should be developed to address the question of the existence of long term ionospheric trends; Ulich *et al.* (2003) stress that to make any trends believable, a suitable statistical modeling, a proper treatment of "errors and uncertainties" is called for.

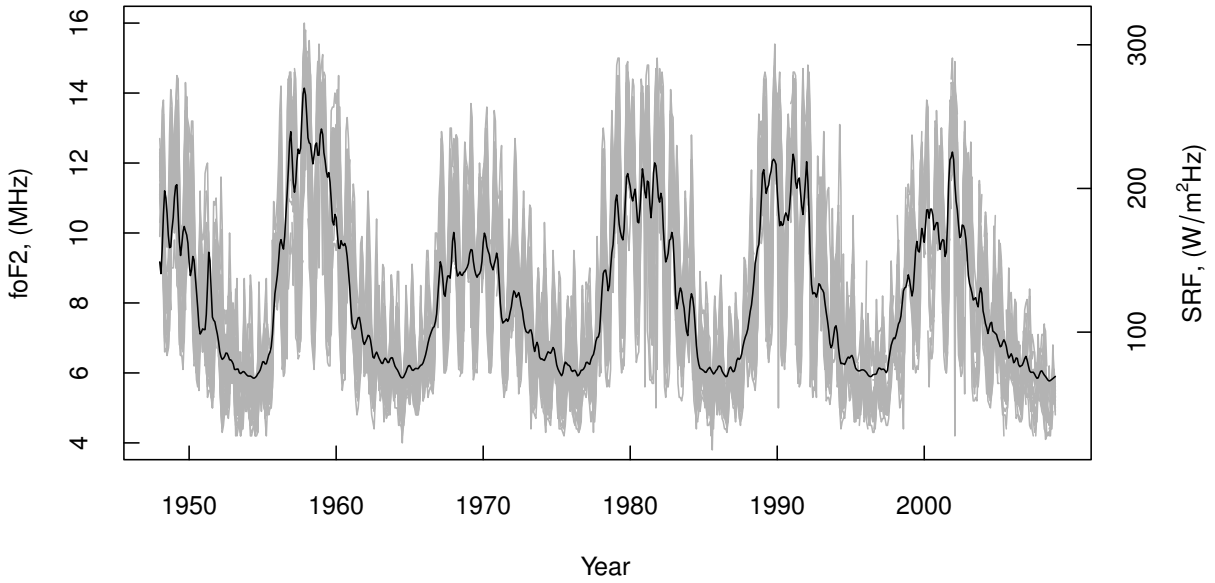

Figure 2: Gray lines represent all foF2 records analysed in this paper with the scale on the left-hand side. The black line represents the observed solar radio flux with the scale on the right-hand side.

Our objective is to make a contribution in this direction which establishes the existence of the negative foF2 trend over the mid–latitude Northern Hemisphere with statistical significance. This is achieved by developing an inferential framework which allows us to combine incomplete ionosonde records from globally distributed locations and take their spatial dependence into account. The absence of complete records has been a major

stumbling block in space physics research to date. Our approach is developed in the framework of functional data analysis: the ionosonde records are viewed as spatially indexed curves which are only partially observed.

There has been an increasing interest in correlated (in particular spatially dependent) functional data. Such data occur in many settings of practical relevance: meteorological and pollution variables at many locations measured over long periods of time, records of brain activity at a number of locations within the brain, economic or health variables indexed by counties, etc. An interested reader is referred to Delicado *et al.* (2010), Giraldo *et al.* (2009, 2011, 2012), Nerini *et al.* (2010), Secchi *et al.* (2011, 2012), Jiang and Serban (2012), Crainiceanu *et al.* (2012), Gromenko *et al.* (2012), Gromenko and Kokoszka (2013, 2012) and Staicu *et al.* (2010, 2012). The work of Liebl (2013) is also related as it considers functions whose domain is not fixed. Even though our new functional regression technique has been developed to solve a specific science problem, it is hoped that it will be received with interest as a more broadly applicable tool of functional data analysis.

The data used in this paper are spatio–temporal. There are two natural ways of looking at them: as a collection of time series at fixed locations (the view we take) or as a time series of geostatistical processes, see e.g. Section 6.4 of Cressie and Wikle (2011). The specific approach to be taken depends on the problem at hand. We want to determine if a collection of time series contains a common linear trend, so the latter approach is more appropriate. If, for example, the temporal evolution of spatial covariances is of interest, the former approach would be more suitable. Spatio–temporal statistic has been a focus of very intense research over the last two decades, with hundreds of important contributions, in addition of the monograph of Cressie and Wikle (2011), Sherman (2010) and Gelfand *et al.* (2010) contain very informative chapters with a large number of references.

The remainder of the paper is organized as follows. In Section 2, we introduce the space physics data we work with. Section 3 is devoted to the new statistical methodology we developed to solve the problem outlined above. Some technical aspects of this methodology are explained in the appendices. In Section 4, we apply these tools to establish, with statistical significance, the existence of a negative foF2 trend in the mid–latitude Northern Hemisphere.

2 The data

To make our conclusions directly comparable to those of Bremer *et al.* (2012), we use the same dataset compiled by Damboldt and Suessmann (2012). This dataset is very new to spatio–temporal statistical community, and adequate attention of statisticians may significantly advance the field of space physics. It contains monthly medians of hourly data for 258 foF2 records and 239 records of the so-called M3000F2 index. Each temporal

record corresponds to a spatial location. Due to various reasons, the records contain long gaps of missing observations. These gaps often appear at the end or the beginning of the record because some stations started operation a decade or two later than others, and some were shut down. In some cases, a station was shut down and reopened many years later. Shorter periods of missing observations are mostly due to equipment maintenance or replacement.

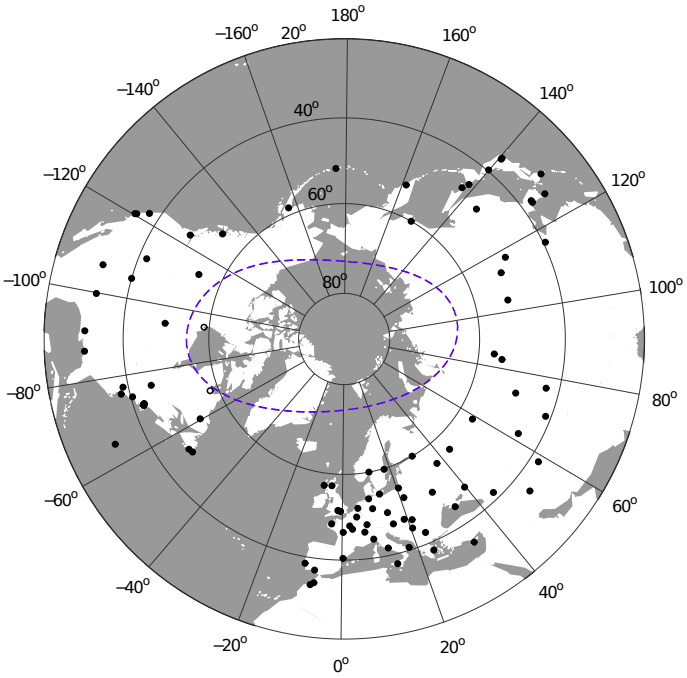

Figure 3: Locations of the 96 ionosonde stations used in this study, black discs. The two circles in northern Canada represent stations located in the auroral zone (dashed line), which were not used.

For the study reported in the paper, we use monthly medians at 12 LT (LT denotes local solar time). At noon, the behavior of the ionosphere is completely dominated by the solar radiation, see Fig. 2, which can be removed using our regression model. At night, the behavior of the ionosphere is complicated, and we postpone the study of the night time data to a more specialized space physics paper. Our statistical study requires the assumption of spatial stationarity. To make this assumption reasonable, we focus

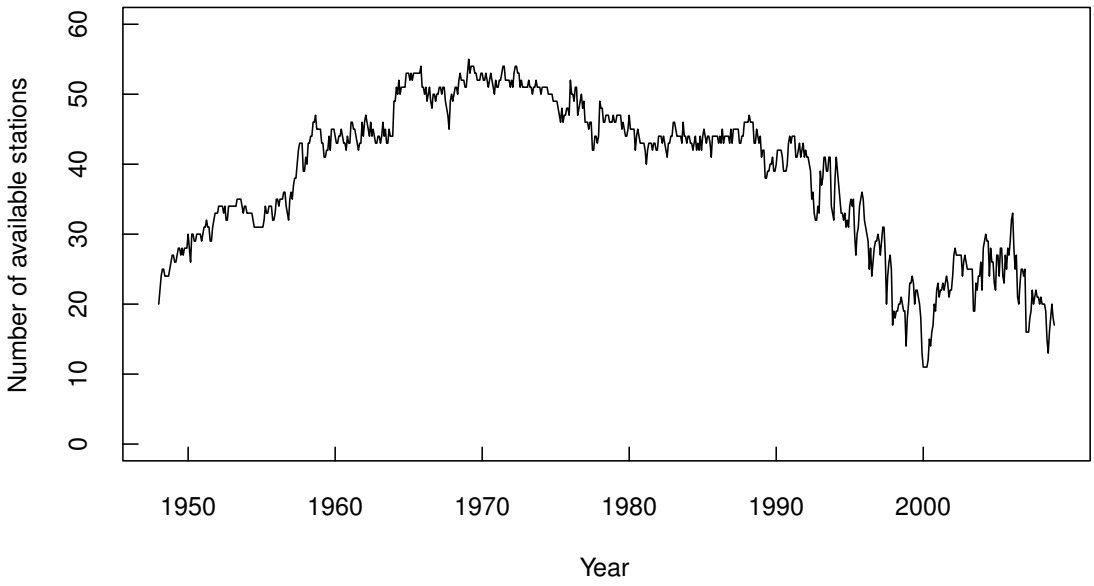

Figure 4: Number of available stations in the mid–latitude northern hemisphere.

only on the mid–latitude region located between 30°N and 60°N geographic latitude. The ionosphere can be divided into three regions, equatorial, mid–latitude and auroral, see Kelly (2009). It exhibits different electron density profiles in each of these regions, with the profile shown in Fig. 1 typical of the mid–latitude region. The reason for choosing the northern hemisphere, rather than the southern hemisphere, is that it contains the longest records with the most extensive spatial coverage, see Fig. 3. We dropped two Canadian stations located between 30°N and 60°N which are however in the auroral zone (determined by the magnetic coordinates). Visual examination shows that these two records indeed appear to be outliers. The total number of selected stations is 96. The majority of the ionosondes started to operate in 1957, the international geophysical year. We selected the time interval from January 1948 to December 2008, so that the total number of months is 732. While the total number of selected stations is 96, the number of stations available at any specific month never exceeds 60, see Fig. 4.

The foF2 curves are used as responses in our functional regression. The main explanatory variable is the observed solar radio flux (SRF), available at the Space Physics Interactive Data Resource (SPIDR), `http://spidr.ngdc.noaa.gov/spidr/`, which is a well established proxy for the solar activity.

3 Statistical model and inference

Let $Y(\mathbf{s}_k;\tau)$ be the original record at location $\mathbf{s}_k$, measured from 1948 to 2008, possibly with missing values. The set of all locations is $\{\mathbf{s}_k, 1 \le k \le K\}$, and the set of time points at which measurements may be available is $\{\tau_i, 1 \le i \le T\}$, in our study these are months from January 1948 to December 2008. We postulate the following functional spatio–temporal model:

$$Y(\mathbf{s};\tau) = \mu(\tau) + \varepsilon(\mathbf{s};\tau) + \theta(\mathbf{s};\tau), \tag{3.1}$$

where $\mathbf{s}$ is a generic location in a region of interest, and τ is continuous time. Our interest lies in the estimation of the mean function $\mu(\cdot)$, and testing if it contains a linear trend. This function does not depend on location; it describes the global upward or downward movement of the F2-region of the ionosphere. The function $\mu(\cdot)$ is treated as an unknown deterministic functional parameter. The second term, $\varepsilon(\mathbf{s};\tau)$, describes the spatio–temporal variability away from the mean function. Stochastic modeling of this term is needed to develop inferential procedures, it will be discussed below. The term $\theta(\mathbf{s};\tau)$ represents a random error, which can be associated with measurement error; the random variables $\theta(\mathbf{s}_k;\tau_i)$ are assumed to be iid and independent of the field $\varepsilon(\cdot,\cdot)$. In our study, due to time aggregation and the precision of the instruments, the estimated variance of the $\theta(\mathbf{s}_k;\tau_i)$ is very small relative to all other terms, and the error term $\theta(\mathbf{s};\tau)$ can be neglected. It could play a much more pronounced role in medical longitudinal studies, in which large measurement errors are common.

In Section 3.1, we explain our approach to modeling the functional spatio–temporal errors $\varepsilon(\mathbf{s};\tau)$, which is needed to understand the procedure for the estimation of the global mean function $\mu(\cdot)$ and to quantify the variability of the estimator. Estimation of $\mu(\cdot)$ is explained in Section 3.2. Section 3.3 focuses on testing if the function $\mu(\cdot)$ contains a linear trend.

3.1 Modeling the field $\varepsilon(\mathbf{s};\tau)$

We split each record into annual subrecords which are denoted by $X_n(\mathbf{s}_k;t_i)$, the index $1 \le n \le N$ denotes year. Time points within a year are denoted $\{t_i,\ 1 \le i \le L\}$, in our study $L = 12$. For a generic location $\mathbf{s}$, we thus have $Y(\mathbf{s};\cdot) = [X_1(\mathbf{s};\cdot) \cup \ldots \cup X_N(\mathbf{s};\cdot)]$. This approach naturally accommodates the annual periodicity of the records. To simplify notation, we assume that the time within a year is rescaled to cover the unit interval $[0,1]$, so that $t \in [0,1]$ and $\tau \in [0,N]$. Each function $X_n(\mathbf{s}_k,\cdot)$ is assumed to be a random

element of the space $L^2 = L^2([0,1])$ such that

$$E\left\|X_n(\mathbf{s}_k,\cdot)\right\|^2 = E\int_0^1 X_n^2(\mathbf{s}_k,t)dt < \infty.$$

Even though we work with 12 observations for each curve $X_n(\mathbf{s}_k,\cdot)$, we view it as a smooth function rather than as a multivariate vector. This is because these curves have pronounced shapes and are not collections of 12 values with an arbitrary covariance structure. The functional approach is applicable to any measurement frequency, e.g. daily or irregular.

We now state assumptions which specify the stochastic structure of the L^2–valued (functional) spatio–temporal field $\{X_n(\mathbf{s}_k,\cdot),\ 1\le n\le N,\ 1\le k\le K\}$.

ASSUMPTION 3.1 *For a fixed year n, the functions $\{X_n(\mathbf{s}_k,\cdot), 1\le k\le K\}$ are realizations of a strictly stationary spatial random field taking values in the space L^2.*

Assumption 3.1 implies that, for a fixed year n, all curves $X_n(\mathbf{s}_k;\cdot)$ have the same distribution in L^2, in particular, they have the same mean function $\mu_n(t) = E[X_n(\mathbf{s},t)]$. In Section 3.2, we impose an additional assumption that

$$\mu_n(t) = \mu(n-1+t),\ t\in[0,1],\quad 1\le n\le N,$$

to ensure that the mean function μ in (3.1) is continuous. In this section we are concerned with the modeling of the covariance structure. The covariance structure of functional data is specified by the covariance operator whose eigenfunctions are the *functional principal components* (FPC's); detailed background is given in Chapters 2 and 3 of Horváth and Kokoszka (2012). Assumption 3.1 implies that each function $X_n(\mathbf{s}_k;\cdot)$ has the same FPC's, which we denote by $v_{nj}(t)$, and so admits the expansion

$$X_n(\mathbf{s}_k;t) = \mu_n(t) + \varepsilon_n(\mathbf{s}_k;t) + \theta_n(\mathbf{s}_k;t),\quad \varepsilon_n(\mathbf{s}_k;t) = \sum_{j=1}^{\infty}\xi_{nj}(\mathbf{s}_k)v_{nj}(t). \tag{3.2}$$

The covariance structure of each field $\varepsilon_n(\cdot;\cdot)$ is restricted by the separability assumption:

ASSUMPTION 3.2 *For each year n, $E\varepsilon_n(\mathbf{s},t) = 0$ and*

$$E[\varepsilon_n(\mathbf{s}_k;t_i)\varepsilon_n(\mathbf{s}_\ell;t_j)] = \Sigma_n(k,\ell)C_n(t_i,j_j),$$

where $\Sigma_n(k,\ell)$ is the spatial and $C_n(t_i,j_j)$ is the temporal covariance.

The spatial and temporal covariance functions in Assumption 3.2 are defined up to mul-

tiplicative constants, so we impose the following identifiability condition:

$$\int C_n(t,t)dt = \sum_{i=1}^{\infty} \lambda_{ni} = 1, \tag{3.3}$$

where $\lambda_{n1} > \lambda_{n2} > \ldots$ are the eigenvalues of the temporal covariance function C_n.

While separability can be criticized as an excessively strong assumption, see e.g. Stein (2005), it is often found acceptable and useful in both theoretical and applied research, see Haas (1995), Genton (2007), Hoff (2011), Paul and Peng (2011), Sun *et al.* (2012), among many others. In our research, we strived to develop a practically applicable and computationally feasible procedure, admittedly at the cost of some simplifying assumptions. We emphasize that the combined error field $\varepsilon(\cdot,\cdot)$ is not separable. It covariance structure is determined by our last assumption.

ASSUMPTION 3.3 *We assume that the fields* $\varepsilon_n(\cdot,\cdot)$, $n \geq 1$, *are independent (but not necessarily identically distributed).*

It is useful to compare the modeling framework described above with our earlier work presented in Gromenko *et al.* (2012) and Gromenko and Kokoszka (2013). In those papers, the error field ε was assumed to be a spatially stationary field of functions in $L^2([0,N])$, no splitting into individual years was done. Such an approach leads to the representation

$$\varepsilon(\mathbf{s};\tau) = \sum_{j=1}^{\infty} \zeta_j(\mathbf{s}) v_j(\tau). \tag{3.4}$$

The new modeling paradigm is dictated by the structure of the data. In Gromenko *et al.* (2012) and Gromenko and Kokoszka (2013) only slightly over 30 locations and a shorter time period were used because extending the spatial and temporal coverage would include many incomplete records (not just missing values but missing decades). The methodology available at that time did not allow us to deal with such records. For example, covariances of the type $\int Y(\mathbf{s}_\ell;\tau)Y(\mathbf{s}_k;\tau)d\tau$ cannot not be computed if the curves $Y(\mathbf{s}_\ell)$ and $Y(\mathbf{s}_k)$ have practically disjoint supports. The methodology described in the remainder of this section allows us to deal with records containing large gaps by using, in a weighted manner, data at neighboring locations. The methods developed in Sections 3.2 and 3.3 can be adapted to errors (3.4). In that case, the fit of the model curves to the observed curves is, however, poor at some locations over certain time intervals. The estimation of the covariance structure, and so the error variances in the trend test, becomes less precise. This point is taken up in more detail in Appendix A.

3.2 Estimation in the presence of incomplete records

We now introduce a new method for the estimation of the mean function $\mu(\cdot)$ and the covariance structure in model (3.1). While the mean function is estimated using the whole period 1948–2008 by combining neighboring curves, the second order structure is estimated using annual records $X_n(\mathbf{s};t)$, separately for each year. This results in a more precise evaluation of errors because the covariances can change with year, a characteristic we observed in the ionosonde data. In our implementation, we use the usual calendar years, but this has no relevance. The point is to account for the annual periodicity due to the rotation around the Sun which changes the angle at which solar radiation impacts the northern hemisphere.

Estimation of the mean function. For complete records, Gromenko *et al.* (2012) and Gromenko and Kokoszka (2013) proposed several approaches. The most straightforward method is to estimate the mean by the weighted sum:

$$\hat{\mu}(\tau) = \sum_{k=1}^{N} w_k Y(\mathbf{s}_k;\tau), \quad \sum_{k=1}^{N} w_k = 1. \tag{3.5}$$

The optimal weights are found by minimizing the expected L^2 distance between the mean and its estimator (3.5), subject to the constraint $\mathbf{w}^T\mathbf{1} = 1$. This leads to the weights: $\mathbf{w} = \mathbf{\Sigma}^{-1}\mathbf{1}/(\mathbf{1}^T\mathbf{\Sigma}^{-1}\mathbf{1})$, where $\mathbf{\Sigma}$ is an $N \times N$ positive definite matrix with entries

$$\Sigma(\mathbf{s}_k,\mathbf{s}_\ell) + \delta_{k\ell}\sigma_\theta^2 = E\int \{Y(\mathbf{s}_k;\tau) - \mu(\tau)\}\{Y(\mathbf{s}_\ell;\tau) - \mu(\tau)\}\,dt. \tag{3.6}$$

It is clear that (3.5) and (3.6) require the curves $Y(\mathbf{s}_k;\tau)$ to be complete. This is particularly important in (3.6); for incomplete records, it may happen that the segments over which $Y(\mathbf{s}_k;\tau)$ and $Y(\mathbf{s}_\ell;\tau)$ are available are practically disjoint. A similar problem occurs if one attempts to use the methods of the estimation of the FPC's v_j in (3.4) developed in Gromenko *et al.* (2012) in situations when large segments of data are missing. These difficulties call for a different approach which we now describe.

Recall that K is the total number of curves, i.e. the number of ionosonde stations used in the study, and the τ_i are the months at which the ionosonde records can, in principle, be available. By $K_i \le K$, we denote the number of observations actually available at month τ_i. To handle the data gaps, the mean function is estimated by the local linear

indexed regression:

$$(\hat{m}_0(\tau), \hat{m}_1(\tau)) = \arg\min_{m_0,m_1} \sum_{i=1}^{T} \kappa_\mu \left(\frac{\tau - \tau_i}{h_\mu} \right) \left\{ \sum_{k=1}^{K_i} w_k(\tau_i) Y(\mathbf{s}_k; \tau_i) - m_0 - m_1(\tau - \tau_i) \right\}^2 . \tag{3.7}$$

The curve $\hat{m}_0(\cdot)$ is the estimate of the mean function $\mu(\cdot)$. We report the results obtained by using the Epanechnikov kernel $\kappa_\mu(t) = 3/4(1 - t^2)\mathbf{1}_{[-1,1]}(t)$ because it has several desirable properties, see e.g. Theorem 3.4 in Fan and Gijbels (1996). Simulations and application to foF2 data show that the choice of the kernel plays practically no role. The conclusions for the foF2 data do not depend on the choice of the bandwidth h_μ either, as long as it is in a reasonable range, so that the smoothed curves visually follow the raw data. Specific values are given in Section 4.

The main idea encapsulated in formula (3.7) is that at each time τ_i we use only the K_i available curves; the weights $w_k(\tau_i)$, which capture the spatial structure, depend on τ_i. Their calculation is discussed in the following. This is a novel aspect because smoothing methodology developed to date, see Yao *et al.* (2005), Yao and Lee (2006), Müller and Yao (2008), assumes independence of the curves.

Calculation of the weights. While we estimate the mean function $\mu(\cdot)$ using the full period 1948-2008, the covariance structure and the weights are estimated for each year separately. Following Gromenko *et al.* (2012), we introduce the *functional variogram*:

$$2\gamma_n(d_{k\ell}) = E\left\{ \int (X_n(\mathbf{s}_k; t) - X_n(\mathbf{s}_\ell; t))^2 dt \right\}.$$

In this paper, $d_{k\ell}$ is the chordal distance between the locations $\mathbf{s}_k$ and $\mathbf{s}_\ell$ on the sphere. A natural estimator of $2\gamma_n(d_{k\ell})$ for *complete records* is

$$2\tilde{\gamma}_n(d_{k\ell}) = \frac{1}{p_{k\ell}} \sum_{P(d_{k\ell})} \frac{1}{L} \sum_{i=1}^{L} (X_n(\mathbf{s}_k; t_i) - X_n(\mathbf{s}_\ell; t_i))^2, \tag{3.8}$$

where $P(d_{k\ell}) = \{(\mathbf{s}_k, \mathbf{s}_\ell) : \|\mathbf{s}_k - \mathbf{s}_\ell\| = d_{k\ell}\}$ and $p_{k\ell}$ is the cardinality of $P(d_{k\ell})$. *The points with $d = 0$ are not included.* When the records are incomplete, averaging over time can be a source of a severe bias especially for short records. Thus, preaveraging over time should be avoided. Instead, we perform averaging for *all available squared differences* $(X_n(\mathbf{s}_k; t_i) - X_n(\mathbf{s}_\ell; t_i))^2$, $1 \le i \le L$, for locations which fall into $P(d_{k\ell})$. The resulting estimator is noisy and the corresponding spatial covariance is not necessarily positive definite. We thus fit a valid parametric semivariogram model to the $\tilde{\gamma}_n(d_{k\ell})$, using nonlinear least squares. For the ionosonde data, we found it sufficient to use the

Gaussian model

$$\gamma_n(d) = (\sigma_n^2 - \sigma_{n\nu}^2)(1 - \exp(-d^2/\rho_n^2)) + \sigma_{n\nu}^2 \mathbf{1}_{(0,\infty)}(d), \tag{3.9}$$

and the Exponential model

$$\gamma_n(d) = (\sigma_n^2 - \sigma_{n\nu}^2)(1 - \exp(-d/\rho_n)) + \sigma_{n\nu}^2 \mathbf{1}_{(0,\infty)}(d). \tag{3.10}$$

Several examples of fitted semivariograms for different years is show in Figure 5. We also fitted the more complex Matern model, which has theoretical advantages, see Stein (1999). However Matern and the Gaussian models produced practically identical fits in terms of RSS. Also, the P-values for the trend test, cf. in Section 4, are very close for both models.

Once the parameters σ_n^2, $\sigma_{n\nu}^2$ and ρ_n^2 have been estimated, calculation of the weights $w_{nk}(t_i)$ is straightforward: we first estimate the covariance matrix $\mathbf{\Sigma}(t_i)$ by plugging in the distances between locations with *available observations* into (3.9) or (3.10) and then use formula

$$\mathbf{w}_n(t_i) = \mathbf{\Sigma}_n(t_i)^{-1}\mathbf{1}/(\mathbf{1}^T\mathbf{\Sigma}_n(t_i)^{-1}\mathbf{1}). \tag{3.11}$$

In (3.11), $\mathbf{\Sigma}_n(t_i)$ is the $K_i \times K_i$ dimensional matrix and $\mathbf{1}$ is the $K_i \times 1$ dimensional vector.

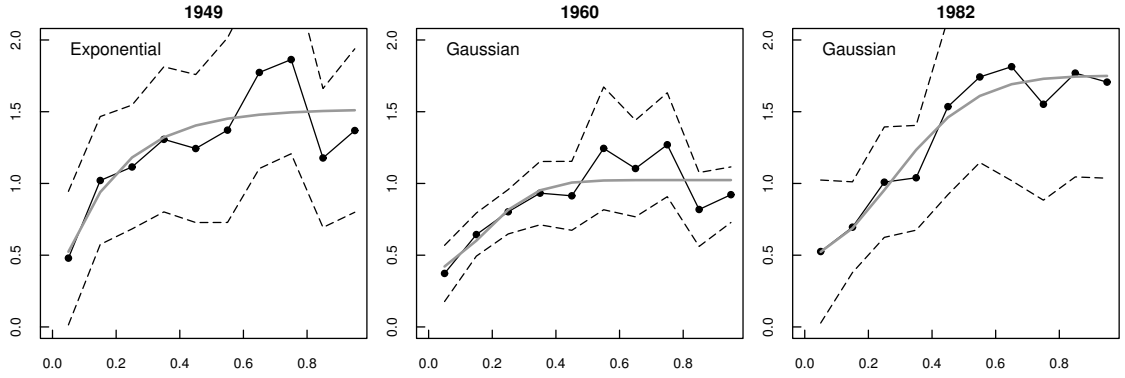

Figure 5: Examples of estimated functional semivariograms for several years. Black lines with dots represent estimated semivariograms with 95% pointwise confidence intervals, dashed lines. Gray lines represent fits to the selected parametric model, captions at corners indicate the selected model. Horizontal axes represent distance in radians.

Estimation of the covariance structure. To determine the statistical significance of the conjectured cooling trend, we need to estimate temporal covariance surface of the incomplete functional field Y. Due to Assumption 3.3 the resulting covariance surface is

block diagonal: $\mathbf{C} = \text{diag}[\mathbf{C}_1, \dots \mathbf{C}_N]$. Before describing our method, we comment the existing covariance surface estimation procedures. When records are independent and fully observed the covariance surface is estimated using the sample covariance function, see e.g. Chapter 2 of Horváth and Kokoszka (2012). When records are correlated and complete, one can use one of the estimators proposed in Gromenko *et al.* (2012), which use projections onto some orthonormal basis. When curves are independent and sparsely observed, the covariance surface may be estimated in a two step procedure proposed in Yao *et al.* (2005). None of the above methods is applicable to our problem which involves incomplete and correlated curves. However, the method of Yao *et al.* (2005) can be extended to take into account spatial dependence. We emphasize that our method assumes equidistant time series perhaps containing missing observations. An extension to spatially dependent curves observed at irregular temporal points remains to be developed. As in Yao *et al.* (2005), we develop a two step procedure. The first step leads to a preliminary estimator for each year which takes into account spatial dependence; the second step is surface smoothing.

For fixed i and j, define the scalar field

$$\psi_n(\mathbf{s}) = (X_n(\mathbf{s}; t_i) - \hat{\mu}_n(t_i))(X_n(\mathbf{s}; t_j) - \hat{\mu}_n(t_j)).$$

By Assumption 3.2, the expectation of $\psi_n(\mathbf{s}_k)$ is approximately equal to $\Sigma_n(k,k)C_n(t_i,t_j)$. For the ease of reading we omit index n. The preliminary temporal covariance surface can be estimated up to a constant as a weighted average

$$\widetilde{C}(t_i, t_j) = \sum_{k=1}^{K} \nu(k)\psi(\mathbf{s}_k), \;\; \sum_{k=1}^{K} \nu(k) = 1.$$

The weights can be selected to minimize the variance of the estimator, which leads to the following solution:

$$\boldsymbol{\nu} = \boldsymbol{\Sigma}_\psi^{-1}\mathbf{1}/(\mathbf{1}^T\boldsymbol{\Sigma}_\psi^{-1}\mathbf{1}) \tag{3.12}$$

where $\boldsymbol{\Sigma}_\psi$ is the covariance matrix with elements $\Sigma_\psi(k,\ell) = \text{Cov}(\psi(\mathbf{s}_k), \psi(\mathbf{s}_\ell))$. The matrix $\boldsymbol{\Sigma}_\psi$ is difficult estimate due to the highly unstable behavior of the spatial field $\psi(\mathbf{s})$. We therefore use the approximation, cf. Appendix B,

$$\text{Cov}(\psi(\mathbf{s}_k), \psi(\mathbf{s}_\ell)) \approx \Sigma^2(k,\ell)g(t_i,t_j), \tag{3.13}$$

i.e. replace in (3.12) the matrix $\boldsymbol{\Sigma}_\psi$ by the matrix $\boldsymbol{\Sigma}^\star$ with entries $\Sigma^2(k,\ell)$. Notice that the multiplication by $g(t_i,t_j)$ in (3.13) plays no role due to the cancelation in (3.12). The entries $\Sigma(k,\ell)$ of the matrix $\boldsymbol{\Sigma}$ are estimated separately for each year using the method

explained in the subsection on the calculation of the weights in (3.7). The measurement noise variance naturally appears in variogram as a nugget and thus automatically included into the spatial covariance Σ.

3.3 Functional regression

Estimation of the trend. Gromenko and Kokoszka (2013) proposed a procedure for determining the linear trend for complete records when all covariates are global, like the SRF which does not depend on the spatial location. Here we generalize that approach to the case of incomplete curves and covariates which may depend on the spatial location. We postulate the model

$$Y(\mathbf{s};\tau) = \sum_{j=1}^{q} \beta_j z_j(\mathbf{s};\tau) + \varepsilon(\mathbf{s};\tau) + \theta(\mathbf{s};\tau), \tag{3.14}$$

keeping in mind that some values $Y(\mathbf{s}_k;\tau_i)$ are not observed. Some covariates are global, i.e. they do not depend on $\mathbf{s}$, but we use the notation $z_i(\mathbf{s};\tau)$ for all of them. All covariates are fully observed and are treated as deterministic regressors.

We now explain how the parameter vector $\boldsymbol{\beta} = [\beta_1, \ldots, \beta_q]^T$ is estimated. Consider the weights (3.11), i.e. those used in the estimation of the mean function by the local regression (3.7). A preliminary estimator $\boldsymbol{\beta}^\star$ is the value of $\boldsymbol{\beta}$ which minimizes

$$\sum_{i=1}^{12N} \left\{ \sum_{k=1}^{K_i} w(\tau_i) \left[Y(\mathbf{s}_k;\tau_i) - \sum_{j=1}^{q} \beta_j z_j(\mathbf{s}_k;\tau_i) \right] \right\}^2. \tag{3.15}$$

To state an explicit formula for the minimizer $\boldsymbol{\beta}^\star$, introduce the vectors

$$\mathbf{z}(\tau_i) = [z_{w1}(\tau_i), z_{w2}(\tau_i), \ldots, z_{wq}(\tau_i)]^T, \qquad z_{wj}(\tau_i) = \sum_{k=1}^{K_i} w_k(\tau_i) z_j(\mathbf{s}_k;\tau_i)$$

and the matrix

$$\mathbf{Q} = \left[\langle z_{wj}, z_{wj'} \rangle \,,\, 1 \le j, j' \le q \right],$$

where

$$\langle z_{wj}, z_{wj'} \rangle = \int_0^N z_{wj}(\tau) z_{wj'}(\tau) d\tau = \frac{1}{12} \sum_{i=1}^{12N} z_{wj}(\tau_i) z_{wj'}(\tau_i).$$

The estimator $\boldsymbol{\beta}^\star$ then has the form

$$\boldsymbol{\beta}^\star = \mathbf{Q}^{-1} \left\langle \mathbf{z}, \mathbf{w}^T \mathbf{Y} \right\rangle, \tag{3.16}$$

where $\left\langle \mathbf{z}, \mathbf{w}^T\mathbf{Y} \right\rangle$ is the $q \times 1$ vector with the jth entry

$$\left\langle \mathbf{z}, \mathbf{w}^T\mathbf{Y} \right\rangle_j = \int_0^N z_{wj}(\tau) \sum_{k=1}^{K(\tau)} w_k(\tau) Y(\mathbf{s}_k; \tau) d\tau = \frac{1}{12} \sum_{i=1}^{12N} z_{wj}(\tau_i) \sum_{k=1}^{K_i} w_k(\tau_i) Y(\mathbf{s}_k; \tau_i).$$

Notice that

$$\mathbf{w}^T\mathbf{Y}(\tau_i) = \sum_{k=1}^{K_i} w_k(\tau_i) Y(\mathbf{s}_k; \tau_i)$$

is the estimate of the mean function μ if no temporal smoothing is used. The final estimator is given by

$$\hat{\boldsymbol{\beta}} = \mathbf{Q}^{-1} \left\langle \mathbf{z}, \hat{\mu} \right\rangle, \qquad \left\langle \mathbf{z}, \hat{\mu} \right\rangle_j = \frac{1}{12} \sum_{i=1}^{12N} z_{wj}(\tau_i) \hat{\mu}(\tau_i), \tag{3.17}$$

where $\hat{\mu}(\tau_i)$ is the estimate obtained using (3.7). The value of $\hat{\boldsymbol{\beta}}$ does not depend on the measurement units for time τ.

Significance of regression coefficients. The variance of the estimator (3.17) is

$$\mathrm{Var}[\hat{\boldsymbol{\beta}}] = \mathbf{Q}^{-1} E\left[\langle \mathbf{z}, \hat{\mu} - E\hat{\mu} \rangle \langle \mathbf{z}, \hat{\mu} - E\hat{\mu} \rangle^T \right] \mathbf{Q}^{-1}, \tag{3.18}$$

where the middle term is a $q \times q$ matrix whose (i, j) element is

$$\iint z_{wi}(t) z_{wj}(t') \mathrm{Cov}(\hat{\mu})(t, t') dt dt'. \tag{3.19}$$

The formula for $\mathrm{Cov}(\hat{\mu})(t, t')$ is lengthy and is given in Appendix C.

Using numerical simulations, we found that the estimator $\hat{\boldsymbol{\beta}}$ is approximately normal even if the functions $X(\mathbf{s}_k)$ are not normally distributed. A heuristic justification of its normality is that it is a weighed sum of a large number of $Y(\mathbf{s}_k, \tau_i)$. In the absence of dependence, the weights would be all equal, and the normality of $\hat{\boldsymbol{\beta}}$ would be a consequence of the central limit theorem. The ionosonde data do not acutally show alarming departures from normality, see Fig. 6, so any weighted sum of the $Y(\mathbf{s}_k, \tau_i)$ can be expected to be normal. Thus to test $\beta_i = 0$, for a fixed i, we assume that the statistic $\hat{\beta}_i / \sqrt{\mathrm{Var}[\hat{\beta}_i]}$ has the standard normal distribution, the P-value is calculated as

$$\text{P-value} = 2\left\{ 1 - \Phi\left(\left| \hat{\beta}_i / \sqrt{\mathrm{Var}[\hat{\beta}_i]} \right| \right) \right\}, \tag{3.20}$$

where $\Phi(\cdot)$ is the standard normal distribution function.

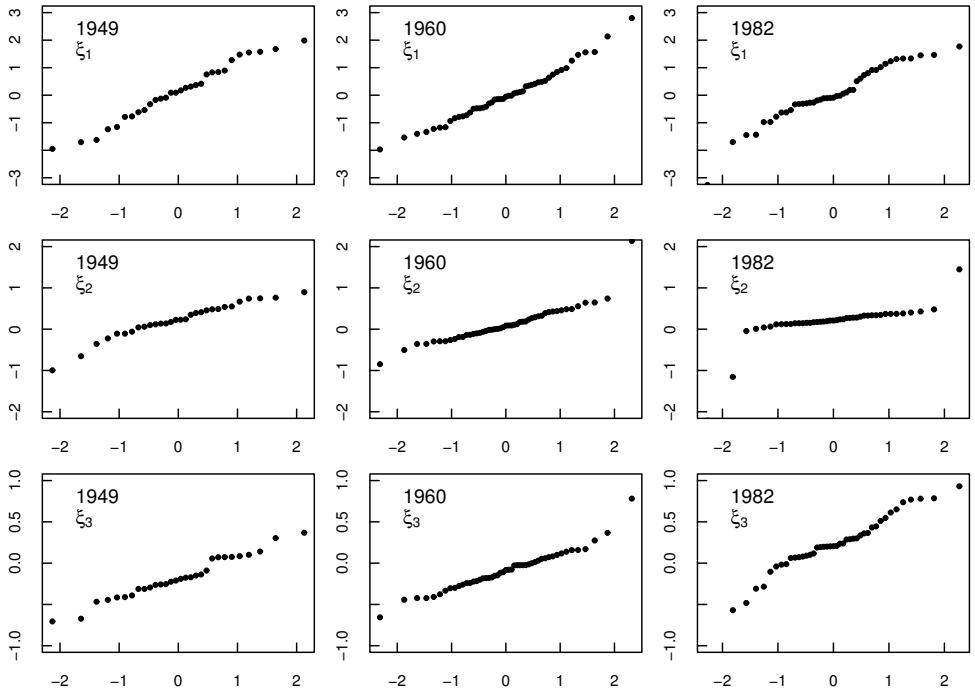

Figure 6: Normal quantile–quantile plots for scores $\boldsymbol{\xi}_1$, $\boldsymbol{\xi}_2$, $\boldsymbol{\xi}_3$ estimated using $h_\mu = 1.5$, cf. (3.2).

4 Application to ionosonde data

We start with exploring the conventional model representing a linear relation between foF2, the solar activity and the postulated trend. In terms of regression (3.14), this model can be written as

$$Y(\mathbf{s}_k;\tau) = \beta_1 + \beta_2\tau + \beta_3\mathrm{SRF}(\tau) + \varepsilon(\mathbf{s}_k;\tau) + \theta(\mathbf{s}_k;\tau), \quad 1 \le k \le 96. \tag{4.1}$$

The global functional covariate SRF is the monthly medians of the observed solar radio flux. Our interest is in estimating the coefficient β_2 and evaluating its statistical significance. Regressions similar to (4.1) have been extensively used in ionospheric research (without splitting the regression errors as $\varepsilon(\mathbf{s}_k;\tau) + \theta(\mathbf{s}_k;\tau)$). In earlier research, an estimate of β_2 would be obtained at a fixed location with a relatively complete record extending over several decades. Its significance would be tested using the usual t–test. The measurements obtained by the Juliusruh (northeastern Germany) ionosonde which started operation in 1961 have been particularly extensively studied. It was however soon observed that the sign and/or significance of β_2 would depend on the location and the time period. In a recent, most comprehensive up to date, study Bremer *et al.* (2012) estimated β_2 practically at all available locations and time periods. Their global analysis uses simple averages of the $\hat{\beta}_2$ available over changing time periods. This leads to a useful global picture, but the significance of such globally averaged trends is difficult to asses in the absence of a statistical model.

We now discuss the the results that follow from the application of our model and testing procedure. Estimates of the linear trend as well as their statistical significance for different smoothing bandwidths h_μ are summarized in Table. 1. The parameter h_μ is measured in months, the temporal averaging thus extends approximately over $1.5h_\mu$ months. Our conclusion (significant negative trend) agrees with the hypothesis of Roble, Dickinson and Rishbeth discussed in Section 1. While a negative trend in the foF2 frequency in the mid–latitude northern hemisphere cannot be quantitatively connected with the magnitute of the hypothesized/observed global warming in the near surface troposphere, there is a strong association due to a common driver: the increased concentration of greenhouse gases. The study of a temporal trend in the ionosphere is easier because there are fewer covariates to be taken into account: the important ones are the solar activity and perhaps the decadal changes in the direction of the internal magnetic field. Terrestrial surface temperature measured at specific locations over a hundred years is impacted by the solar activity but also by many more factors, for example, by urbanization and deforestation, which may produce spurious trends, if not accounted for. The remainder of this section is devoted to the validation of our conclusion by considering refinements of the standard model (4.1).

Exploratory analysis has revealed that the linear term $\beta_1 + \beta_2\tau + \beta_3\mathrm{SRF}(\tau)$ in model

Table 1: Trends and P-values for different bandwidths obtained using model (4.1).

h_μ	$\beta_2, 10^{-3}$MHz/Year	Statistic	P-value
1.5	-1.019 ± 0.439	-2.322	0.02021
2.0	-1.070 ± 0.435	-2.459	0.01393
2.5	-0.965 ± 0.414	-2.328	0.01993
3.0	-0.945 ± 0.406	-2.331	0.01975
3.5	-1.083 ± 0.387	-2.799	0.00513
4.0	-1.150 ± 0.378	-3.045	0.00232
4.5	-1.243 ± 0.364	-3.416	0.00063
5.0	-1.291 ± 0.356	-3.628	0.00039

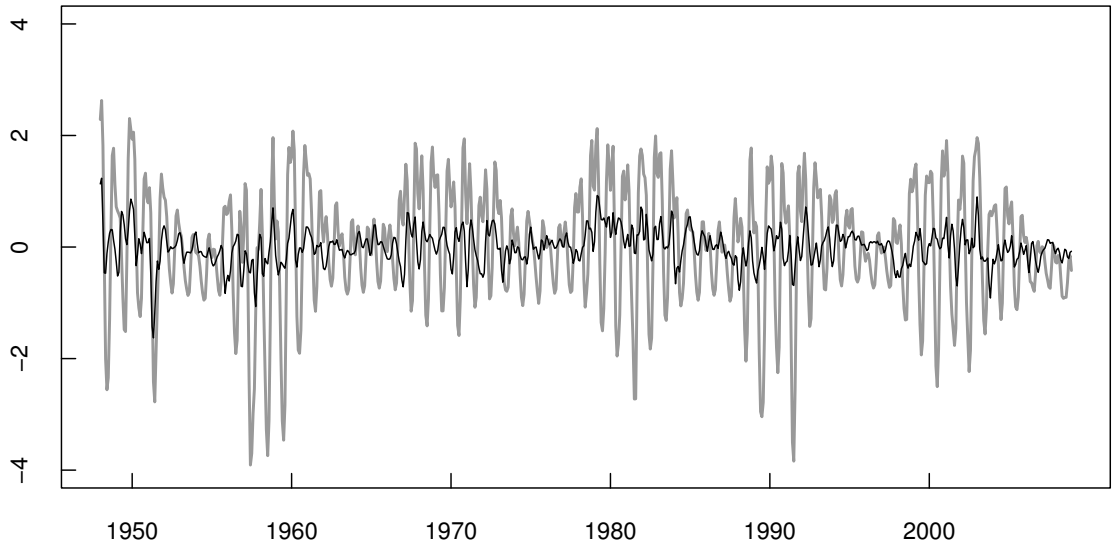

Figure 7: Gray line shows the difference $\hat{\mu}(\tau) - (\hat{\beta}_1 + \hat{\beta}_2\tau + \hat{\beta}_3\text{SRF}(\tau))$. Black line shows the difference $\hat{\mu}(\tau) - (\hat{\beta}_1 + \hat{\beta}_2\tau + \hat{\beta}_3\hat{z}_3^{\text{eff}}(\tau))$.

(4.1) does not accurately represent the nonparametrically estimated mean, $\hat{\mu}(\tau)$. The difference $\hat{\mu}(\tau) - (\beta_1 + \beta_2\tau + \beta_3\text{SRF}(\tau))$ is quite large and has a very strong annual dependence, see Fig. 7. The main reason for the annual variation in the difference is due to the change in zenith angle θ_Z which affects the effective solar radio flux. Exploratory analysis has shown that the covariate

$$z_3^{\text{eff}}(\tau) = a_1(\tau) + a_2(\tau)\ln(\text{SRF}(\tau)),$$

where coefficients $a_1(\tau)$ and $a_2(\tau)$ depend on the time of a year but not a year itself,

Table 2: Trends and P-values for different bandwidths obtained using model (4.2).

h_μ	$\beta_2, 10^{-3}$MHz/Year	Statistic	P-value
1.5	-2.179 ± 0.438	-4.977	$6.461 \cdot 10^{-7}$
2.0	-2.224 ± 0.434	-5.118	$3.082 \cdot 10^{-7}$
2.5	-1.951 ± 0.414	-4.714	$2.425 \cdot 10^{-6}$
3.0	-1.871 ± 0.405	-4.619	$3.861 \cdot 10^{-6}$
3.5	-1.826 ± 0.387	-4.720	$2.356 \cdot 10^{-6}$
4.0	-1.810 ± 0.378	-4.797	$1.609 \cdot 10^{-6}$
4.5	-1.736 ± 0.364	-4.773	$1.816 \cdot 10^{-6}$
5.0	-1.699 ± 0.356	-4.776	$1.786 \cdot 10^{-6}$

resembles the estimated mean $\hat{\mu}(\tau)$ much better than $\beta_1 + \beta_3 \mathrm{SRF}(\tau)$. The association between $\hat{\mu}(\tau)$ and $z_3^{\mathrm{eff}}(\tau)$ is linear and the correlation is very close to one for different months. The estimated difference $\hat{\mu}(\tau) - \hat{z}_3^{\mathrm{eff}}(\tau)$ exhibits a much weaker seasonal dependence, see Fig. 7. For a more accurate analysis we therefore recommend the following model

$$Y(\mathbf{s}_k;\tau) = \beta_1(\tau) + \beta_2\tau + \beta_3\hat{z}_3^{\mathrm{eff}}(\tau) + \varepsilon(\mathbf{s}_k;\tau) + \theta(\mathbf{s}_k;\tau), \quad 1 \le k \le 96, \tag{4.2}$$

The regressor $\hat{z}_3^{\mathrm{eff}}(\tau)$ can be estimated precisely, and we can use the same methodology as before for estimating the linear trend parameter β_2. The $\hat{\beta}_2$'s for model (4.2) and the corresponding P–values are reported in Table. 2. The estimated trend in model (4.2) is larger in absolute terms than in model (4.1) and the P–values are correspondingly smaller. We thus see that using a more precise proxy for the solar activity, which also takes into account annual changes in the the zenith angle, confirms our conclusion, which is seen to be robust to the form the solar activity proxy.

As Bremer *et al.* (2012), we now show how the conclusion depends on the total length of the time interval used in the estimation and testing. To do this, we fix the interval length, L, and determine the trend for all possible intervals of length L. Fig. 8 shows signs of estimated trends as well as their statistical significance. Both models (4.1) and (4.2) provide qualitatively the same result. There is a region around 1960 which, when included into the estimation interval, tends to make the trend positive. However, one gets consistently negative trend when considering interval roughly from 1960 to 2008. A similar observation was made by Bremer *et al.* (2012) using exploratory analysis. It indicates that the negative trend may have an anthropogenic origin.

We also checked the robustness of our conclusion against the inclusion of a local covariate reflecting the potential impact of decadal changes in the direction of the internal

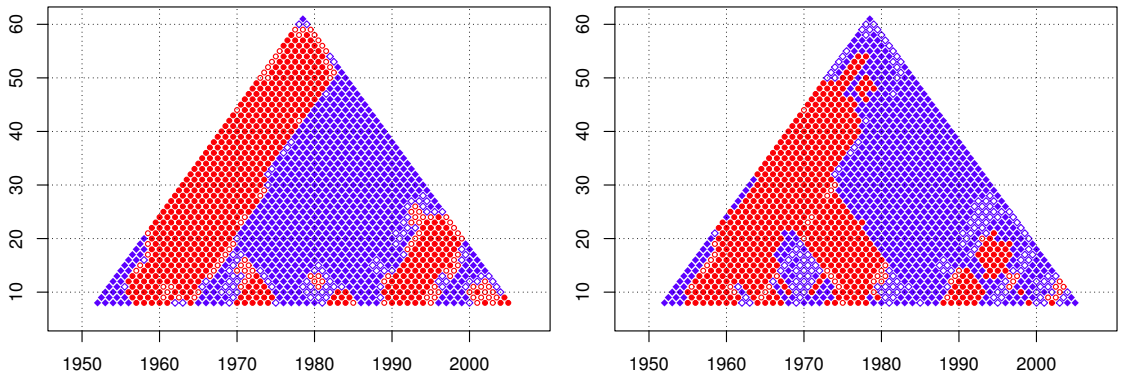

Figure 8: Vertical axes represent the length of a time interval for trend determination in years, horizontal axes represent the position of the *center* of a time interval in years. Blue diamonds represent negative statistically significant trends, blue empty diamonds represent negative insignificant trends, red disks represent positive statistically significant rends, and red circles represent positive statistically insignificant trends. Left panel: Model (4.1). Right panel: Model (4.2).

magnetic field of the Earth. We thus tested the significance of β_2 in the regression

$$Y(\mathbf{s}_k;\tau) = \beta_1 + \beta_2\tau + \beta_3 \mathrm{SRF}(\tau) + \beta_4 M(\mathbf{s}_k;\tau) + \varepsilon(\mathbf{s}_k;\tau) + \theta(\mathbf{s}_k;\tau),$$

where $M(\mathbf{s}_k)$ are given by $M(\mathbf{s}_k;\tau) = \sin I(\mathbf{s}_k;\tau)\cos I(\mathbf{s}_k;\tau)$, where $I(\mathbf{s}_k;\tau)$ is the inclination of the Earth's magnetic field, see e.g. Chapter 13 of Kivelson and Russell (1997) and Elias (2009). This extension led to the values of $\hat{\beta}_2$ and the corresponding P–values similar to those in Table 1, in most cases slightly decreasing the magnitude of the trend and increasing the P-values, but not beyond the 5 percent significance level (for the full 61 year long period).

Appendices

A Error modeling by annually updated covariance estimation

We argued in Section 3.1 that splitting entire temporal records into annual subrecords reduces model errors. A natural justification is that such a split is based on the annual periodicity present in these records beyond the dominant semiperiodicity due to the solar cycle. In principle, the data could be split into segments of 2, 3, etc. years. In this appendix, we provide a quantitative justification that using any period longer that one year decreases the quality of the approximation of the observed curves by curves reconstructed from the model.

Based on (3.2), we can model the ionosonde records as follows

$$\hat{X}_n(\mathbf{s}_k; t) = \hat{\mu}_n(t) + \sum_{j=1}^{p} \hat{\xi}_{nj}(\mathbf{s}_k)\hat{v}_{nj}(t),$$

where now the index n may refer to any period whose length is 1,2, 3, etc. years. The scores ξ_{nj} are estimated conditionally, see Eq (5) in Yao *et al.* (2005) or Chapter 3.2 in Mardia *et al.* (1979). The calculation of the EFPC's $\hat{v}_{nj}$ requires covariance surface estimation. The number of the FPC's p is selected to capture the required level of the cumulative variance. Then we calculate the average approximation squared error

$$R = \sum_{n,k,i} (X_n(\mathbf{s}_k; t_i) - \hat{X}_n(\mathbf{s}_k; t_i))^2 / N_0,$$

where N_0 is the total number of available scalar observations. The resulting errors R for different splittings, different smoothing bandwidths h_μ and different captured cumulative variances are reported in Table 3. It is clear that splitting into one year long intervals provides optimal approximation to real data.

B Derivation of approximation (3.13)

Approximation (3.13) holds if the random variables $X(\mathbf{s}_k; t_i) - \hat{\mu}(t_i),\ 1 \le k \le K,\ 1 \le i \le L$ are approximately mean zero multivariate normal, so that Isserlis' theorem can be applied. Begin with the usual decomposition:

$$\mathrm{Cov}(\psi(\mathbf{s}_k), \psi(\mathbf{s}_\ell)) = E(\psi(\mathbf{s}_k)\psi(\mathbf{s}_\ell)) - E(\psi(\mathbf{s}_k))E(\psi(\mathbf{s}_\ell)).$$

Table 3: Average interpolation errors for multiples of 12 months, different smoothing bandwidths h_μ and different cumulative variances.

	$h_\mu = 1.5$					$h_\mu = 2$				
	80%	85%	90%	95%	99%	80%	85%	90%	95%	99%
12	0.3183	0.3131	0.3100	0.3081	0.3073	0.3279	0.3220	0.3188	0.3168	0.3159
24	0.3404	0.3354	0.3333	0.3317	0.3311	0.3501	0.3452	0.3428	0.3412	0.3405
48	0.3591	0.3571	0.3550	0.3537	0.3532	0.3694	0.3673	0.3652	0.3638	0.3632
72	0.3709	0.3687	0.3671	0.3660	0.3656	0.3812	0.3789	0.3773	0.3763	0.3758
120	0.3772	0.3752	0.3737	0.3728	0.3724	0.3886	0.3860	0.3845	0.3836	0.3832
	$h_\mu = 2.5$					$h_\mu = 3$				
	80%	85%	90%	95%	99%	80%	85%	90%	95%	99%
12	0.3550	0.3470	0.3429	0.3401	0.3391	0.3544	0.3477	0.3420	0.3391	0.3381
24	0.3822	0.3751	0.3716	0.3696	0.3688	0.3836	0.3755	0.3720	0.3698	0.3688
48	0.4088	0.4026	0.4000	0.3983	0.3976	0.4120	0.4050	0.4023	0.4007	0.4000
72	0.4208	0.4173	0.4150	0.4134	0.4128	0.4276	0.4216	0.4188	0.4172	0.4166
120	0.4327	0.4299	0.4276	0.4264	0.4259	0.4395	0.4364	0.4343	0.4328	0.4323
	$h_\mu = 3.5$					$h_\mu = 4$				
	80%	85%	90%	95%	99%	80%	85%	90%	95%	99%
12	0.3452	0.3393	0.3331	0.3293	0.3277	0.3632	0.3585	0.3520	0.3479	0.3464
24	0.3664	0.3610	0.3553	0.3519	0.3509	0.3661	0.3629	0.3555	0.3524	0.3513
48	0.3935	0.3876	0.3841	0.3815	0.3806	0.3867	0.3824	0.3759	0.3733	0.3723
72	0.4123	0.4065	0.4037	0.4012	0.4005	0.4043	0.3982	0.3943	0.3917	0.3910
120	0.4280	0.4223	0.4192	0.4176	0.4170	0.4095	0.4042	0.4015	0.3995	0.3989
	$h_\mu = 4.5$					$h_\mu = 5$				
	80%	85%	90%	95%	99%	80%	85%	90%	95%	99%
12	0.5073	0.5066	0.4992	0.4939	0.4923	0.7276	0.7273	0.7204	0.7153	0.7139
24	0.4310	0.4297	0.4222	0.4188	0.4176	0.5523	0.5515	0.5454	0.5412	0.5404
48	0.4204	0.4166	0.4112	0.4077	0.4066	0.5042	0.5023	0.4948	0.4917	0.4906
72	0.4175	0.4135	0.4081	0.4055	0.4046	0.4690	0.4658	0.4607	0.4578	0.4569
120	0.3839	0.3780	0.3745	0.3729	0.3725	0.3820	0.3794	0.3736	0.3723	0.3720

The second term on the RHS is

$$E(\psi(\mathbf{s}_k))E(\psi(\mathbf{s}_\ell)) = \Sigma(k,k)\Sigma(\ell,\ell)C^2(t_i,t_j),$$

and the first term can be calculated using Isserlis' theorem:

$$\begin{aligned} E(\psi(\mathbf{s}_k)\psi(\mathbf{s}_\ell)) =& \Sigma(k,k)\Sigma(\ell,\ell)C^2(t_i,t_j) \\ &+ \Sigma^2(k,\ell)C(t_i,t_i)C(t_j,t_j) \\ &+ \Sigma^2(k,\ell)C^2(t_i,t_j). \end{aligned}$$

This leads to

$$\mathrm{Cov}(\psi(\mathbf{s}_k),\psi(\mathbf{s}_\ell)) = \Sigma^2(k,\ell)g(t_i,t_j)$$

with $g(t_i,t_j) = C(t_i,t_i)C(t_j,t_j) - C^2(t_i,t_j)$.

C Covariances of the estimated mean function

Everywhere below we assume that the sampling variability of the weights $w_k(t)$ can be neglected. Without this assumptions it is difficult to derive usable expressions.

We introduce the following vectors and matrices, with their dimensions given in parenthesis to facilitate the understanding:

$$\boldsymbol{\mu}_w = \left[\sum_{k=1}^{K_1} w_k(\tau_1)Y(\mathbf{s}_k;\tau_1), \ldots, \sum_{k=1}^{K_T} w_k(\tau_T)Y(\mathbf{s}_k;\tau_T)\right]^T, \quad (T\times 1);$$

$$\mathbf{m}(\tau) = [m_0(\tau), m_1(\tau)]^T, \quad (2\times 1)$$

$$\mathbf{Z}(\tau) = \begin{bmatrix} 1 & \tau-\tau_1 \\ \vdots & \vdots \\ 1 & \tau-\tau_T \end{bmatrix}, \quad (T\times 2);$$

$$\mathbf{K}(\tau) = \mathrm{diag}\left[\kappa((\tau-\tau_1)/h_\mu), \ldots, \kappa((\tau-\tau_T)/h_\mu)\right], \quad (T\times T).$$

Note that $\mathbf{K}(\tau)$, $\mathbf{Z}(\tau)$ and $\mathbf{m}(\tau)$ depend on continuous τ, while $\boldsymbol{\mu}_w$ is a vector of a fixed length.

The solution to (3.7) has the form

$$\hat{\mathbf{m}}(\tau) = \mathbf{A}^{-1}(\tau)\mathbf{Z}^T(\tau)\mathbf{K}(\tau)\boldsymbol{\mu}_w, \tag{C.1}$$

where $\mathbf{A}(\tau) = \mathbf{Z}^T(\tau)\mathbf{K}(\tau)\mathbf{Z}(\tau)$ is a 2×2 symmetric matrix. The covariance matrix of $\hat{\mathbf{m}}(\tau)$ is equal to

$$\mathrm{Cov}(\hat{\mathbf{m}})(\tau,\tau') = \mathbf{A}^{-1}(\tau)\mathbf{Z}^T(\tau)\mathbf{K}(\tau)\mathrm{Cov}(\boldsymbol{\mu}_w,\boldsymbol{\mu}_w^T)\mathbf{K}(\tau')\mathbf{Z}(\tau')\mathbf{A}^{-1}(\tau'). \tag{C.2}$$

Thus the covariances of the mean function are

$$\text{Cov}(\hat{\mu})(\tau,\tau') = e_1^T \text{Cov}(\hat{\mathbf{m}})(\tau,\tau') e_1, \tag{C.3}$$

where $e_1 = [1,0]^T$.

The only factor in (C.2) that requires attention is $\text{Cov}(\boldsymbol{\mu}_w, \boldsymbol{\mu}_w^T)$ which is a $T \times T$ matrix. To calculate it in a general setting with measurement error we use model (3.2). Treating the weights w_k as fixed, we obtain

$$\text{Cov}(\boldsymbol{\mu}_w(\tau_i), \boldsymbol{\mu}_w(\tau_j)) = \begin{cases} \sum_{k=1}^{K_i} \sum_{\ell=1}^{K_j} w_k(\tau_i) w_\ell(\tau_j) \Sigma_n(k,\ell) C_n(\tau_i,\tau_j), & |i-j| \le 12 \\ 0, & \text{otherwise,} \end{cases} \tag{C.4}$$

where $n = i \bmod 12$.

Notice that formula (C.2) is computationally intensive.

References

Bremer, J., Damboldt, T., Mielich, J. and Suessmann, P. (2012). Comparing long–term trends in the ionospheric F2–region with two different methods. *Journal of Atmospheric and Solar–Terrestrial Physics*, **77,** 174–185.

Crainiceanu, C. M., Staicu, A. M., Ray, S. and Punjabi, N. (2012). Bootstrap-based inference on the difference in the means of two correlated functional processes. *Statistics in Medicine*, **31,** 3223–3240.

Cressie, N. and Wikle, C.K. (2011). *Statistics for Spatio-Temporal Data*. Wiley, Hoboken.

Damboldt, T. and Suessmann, P. (2012). Consolidated database of worldwide measured monthly medians of ionospheric characteristics foF2 and M(3000)F2. *INAG Bulletin on the Web* I, **NAG-73,**; `www.ips.gov.au/IPSHosted/INAG/web-73/index.html`.

Delicado, P., Giraldo, R., Comas, C. and Mateu, J. (2010). Statistics for spatial functional data: some recent contributions. *Environmetrics*, **21,** 224–239.

Elias, A.G. (2009). Trends in the F2 ionospheric layer due to long-term variations in the Earth's magnetic field. *Journal of Atmospheric and Solar-Terrestrial Physics*, **71,** 1602–1609.

Fan, J. and Gijbels, I. (1996). *Local Polynomial Modelling and its Applications*. Chapman & Hall/CRC, London.

Gelfand, A.E., Diggle, P., Guttorp, P. and Fuentes, M. (2010) (eds). *Handbook of Spatial Statistics*. Chapman & Hall/CRC.

Genton, M. G. (2007). Separable approximations of space-time covariance matrices. *Environmetrics*, **18,** 681–695.

Giraldo, R., Delicado, P. and Mateu, J. (2009). Continuous time–varying kriging for spatial prediction of functional data: an environmental application. *Journal of Agricultural, Biological, and Environmental Statistics*, **15,** 66–82.

Giraldo, R., Delicado, P. and Mateu, J. (2011). Ordinary kriging for function–valued spatial data. *Environmental and Ecological Statistics*, **18,** 411–426.

Giraldo, R., Delicado, P. and Mateu, J. (2012). Hierarchical clustering of spatially correlated functional data. *Statistica Neerlandica*, **66,** 403–421.

Gromenko, O. and Kokoszka, P. (2012). Testing the equality of mean functions of ionospheric critical frequency curves. *Journal of the Royal Statistical Society: Series C*, **61,** 715–731.

Gromenko, O. and Kokoszka, P. (2013). Nonparametric inference in small data sets of spatially indexed curves with application to ionospheric trend determination. *Computational Statistics and Data Analysis*, **59,** 82–94.

Gromenko, O., Kokoszka, P., Zhu, L. and Sojka, J. (2012). Estimation and testing for spatially indexed curves with application to ionospheric and magnetic field trends. *The Annals of Applied Statistics*, **6,** 669–696.

Haas, T. C. (1995). Local Prediction of a Spatio-Temporal Process with an Application to Wet Sulfate Deposition. *Journal of the American Statistical Association*, **90,** 1189–1199.

Hoff, P. D. (2011). Separable covariance arrays via the tucker product, with applications to multivariate relational data. *Bayesian Analysis*, **6,** 179–196.

Horváth, L. and Kokoszka, P. (2012). *Inference for Functional Data with Applications*. Springer, New York.

Jiang, H. and Serban, N. (2012). Clustering random curves under spatial interdependence with application to service accessibility. *Technometrics*, **54,** 108–137; With discussion.

Kelly, M. C. (2009). *The Earth's Ionosphere*, 2nd edn. Academic Press, San Diego.

Kivelson, M. G. and Russell, C. T. (1997) (eds). *Introduction to Space Physics*. Cambridge University Press, Cambridge.

Lastovicka, J., A, V. Mikhailov, Ulich, T., Bremer, J., Elias, A., Ortiz de Adler, N., Jara, V., Abbarca del Rio, R., Foppiano, A., Ovalle, E. and Danilov, A. (2006). Long term trends in foF2: a comparison of various methods. *Journal of Atmospheric and Solar-Terrestrial Physics*, **68,** 1854–1870.

Lastovicka, J., Akmaev, R. A., Beig, G., Bremer, J., Emmert, J. T., Jacobi, C., Jarvis, J. M., Nedoluha, G., Portnyagin, Yu. I. and Ulich, T. (2008). Emerging pattern of global change in the upper atmosphere and ionosphere. *Annales Geophysicae*, **26,** 1255–1268.

Liebl, D. (2013). Modeling and forecasting electricity spot prices: a functional data perspective. *The Annals of Applied Statistics*, **7,** 1562–1592.

Mardia, K. V., Kent, J. T. and Bibby, J. M. (1979). *Multivariate analysis*. Academic Press, San Diego.

Mielich, J. and Bremer, J. (2013). Long-term trends in the ionospheric F2 region with different solar activity indices. *Annals of Geophysics*, **31,** 291–303.

Müller, H-G. and Yao, F. (2008). Functional additive models. *Journal of the American Statistical Association*, **103,** 1534–1544.

Nerini, D., Monestiez, P. and Mantéa, C. (2010). Cokriging for spatial functional data. *Journal of Multivariate Analysis*, **101,** 409–418.

Paul, D. and Peng, J. (2011). Principal components analysis for sparsely observed correlated functional data using a kernel smoothing approach. *Electronic Journal of Statistics*, **5,** 1960–2003.

Rishbeth, H. (1990). A greenhouse effect in the ionosphere? *Planetary and Space Science*, **38,** 945–948.

Roble, R. G. and Dickinson, R. E. (1989). How will changes in carbon dioxide and methane modify the mean structure of the mesosphere and thermosphere? *Geophysical Research Letters*, **16,** 1441–1444.

Secchi, P., Vantini, S. and Vitelli, V. (2011). A clustering algorithm for spatially dependent functional data. *Procedia Environmental Sciences*, **7,** 176–181.

Secchi, P., Vantini, S. and Vitelli, V. (2012). Bagging Voronoi classifiers for clustering spatial functional data. *International Journal of Applied Earth Observation and Geoinformation*, **22,** 53–64.

Sherman, M. (2010). *Spatial Statistics and Spatio–Temporal Data*. Wiley.

Staicu, A-M., Crainiceanu, C. and Carroll, R. J. (2010). Fast methods for spatially correlated multilevel functional data. *Biostatistics*, **11,** 177–194.

Staicu, A. M., Crainiceanu, C. M., Reich, D. S. and Ruppert, D. (2012). Modeling functional data with spatially heterogeneous shape characteristics. *Biometrics*, **68,** 331–343.

Stein, M. L. (1999). *Interpolation of Spatial Data: Some Theory for Krigging*. Springer.

Stein, M. L. (2005). Space–time covariance functions. *Journal of the American Statistical Association*, **100,** 310–321.

Sun, Y., Li, B. and Genton, M.G. (2012). Geostatistics for large datasets. In *Advances and Challenges in Space-time Modelling of Natural Events*, *Berlin* (eds E. Porcu, J.M. Montero and M. Schlather), chapter 3, pp. 55–77. Springer.

Ulich, T., Clilverd, M. A. and Rishbeth, H. (2003). Determining long-term change in the ionosphere. *Eos, Transactions American Geophysical Union*, **84,** 581–585.

Yao, F. and Lee, T. (2006). Penalized spline models for functional principal component analysis. *Journal of the Royal Statistical Society: Series* B, **68,** 3–25.

Yao, F., Müller, H-G. and Wang, J-L. (2005). Functional data analysis for sparse longitudinal data. *Journal of the American Statistical Association*, **100,** 577–590.